

# M2H-MX: Multi-Task Semantic and Geometric Perception for Real-Time Monocular 3D Scene Graph Construction

U.V.B.L. Udugama<sup>1</sup>, George Vosselman<sup>1</sup>, and Francesco Nex<sup>1</sup>

**Abstract**—Monocular cameras are attractive for robotic perception because they are lightweight, low-cost, and easy to deploy. However, real-time spatial understanding from a single RGB stream remains difficult because metric geometry, semantic consistency, inference latency, and mapping stability are tightly coupled. This paper presents M2H-MX, a deployment-oriented multi-task front end that combines a frozen foundation-model encoder with lightweight adaptation, register-gated global context, and controlled cross-task refinement. Its predictions are converted through a compact perception-to-mapping interface into inputs for a fixed mapping pipeline, enabling metric-semantic mapping and downstream 3D scene graph construction. On NYUDv2, M2H-MX-L achieves the best performance among the compared multi-task baselines, improving semantic mIoU by 4.06 points and reducing depth RMSE by 9.4%. Runtime evaluation on an NVIDIA RTX 4080 Super shows that the full asynchronous perception-to-mapping loop sustains 15–20 Hz. On ScanNet, M2H-MX reduces average trajectory error by 60.7% compared with a strong monocular SLAM baseline while producing cleaner metric-semantic maps. These results show that dense multi-task perception can provide measurable system-level gains for monocular robotic mapping.

**Index Terms**—Dense Prediction, Multi-task Learning, Real-Time Perception, Monocular SLAM, Semantic Mapping

## I. INTRODUCTION

MONOCULAR cameras are widely used in robotics because they are compact, inexpensive, and simple to integrate. Yet, reliable spatial understanding from a single RGB stream remains challenging. A robot must recover metric geometry, semantic labels, and stable map updates from ambiguous monocular observations, while still operating within the latency budget of real-time mapping and planning. As a result, many spatial mapping systems continue to rely on RGB-D or LiDAR sensors, or on dense perception models that are too expensive for practical monocular deployment.

This work examines how much a stronger dense perception front end can improve a monocular mapping system when the remaining pipeline is kept fixed. We use a Mono-Hydra-based pipeline [1], building on metric-semantic mapping systems such as Kimera [2] and Hydra [3]. The state estimation, mapping, optimization, and scene graph construction modules are kept unchanged; M2H-MX replaces only the dense monocular perception front end by providing predicted metric depth and semantic labels from RGB input.

<sup>1</sup>All authors are with the Department of Earth Observation Science, University of Twente, Enschede, 7522 NH, The Netherlands. {b.udugama, george.vosselman, f.nex}@utwente.nl

M2H-MX available at [https://github.com/BavanthaU/m2h\\_mx](https://github.com/BavanthaU/m2h_mx).

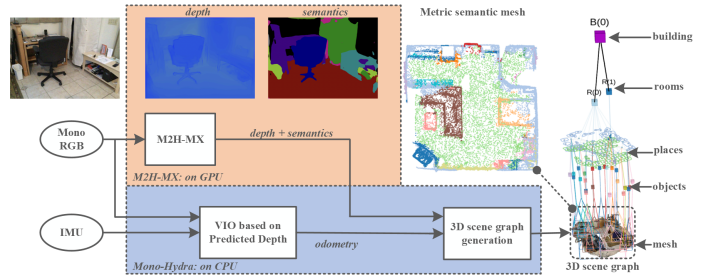


Fig. 1. System overview of M2H-MX as a GPU-based perception front end to the fixed Mono-Hydra [1] monocular SLAM pipeline. From monocular RGB input, M2H-MX predicts dense depth and semantic labels that are consumed by CPU-based RGB-D inertial odometry and mapping. The shown pipeline example uses ScanNet scene0000\_00.

Using learned monocular perception inside this loop imposes constraints that are often hidden in standalone dense prediction benchmarks. The predictions must be accurate, fast enough to avoid blocking the mapping backend, stable enough to support tracking and map fusion, and compatible with the interface expected by the SLAM system. Recent multi-task dense prediction methods improve monocular depth and semantic segmentation by sharing complementary cues [4]–[6], while metric-semantic maps and scene graphs provide structured representations for robot reasoning [2], [3]. However, how modern dense prediction models should be designed and evaluated for real-time monocular mapping remains underexplored.

This paper addresses this gap with M2H-MX, a dense monocular perception module designed for real-time metric-semantic mapping and spatial understanding. Its design is guided by deployment constraints: preserving strong foundation-model features, controlling cross-task interference, and maintaining stable runtime behavior. The main contributions are:

- We introduce **M2H-MX**, a deployment-oriented monocular spatial perception framework that predicts metric depth and semantic labels from RGB images while balancing accuracy, cross-task consistency, and real-time operation.
- We propose a **compact perception-to-mapping interface** that uses predicted depth and semantic cues to support visual-inertial odometry, metric-semantic mapping, and downstream **3D scene graph** generation from monocular RGB input.

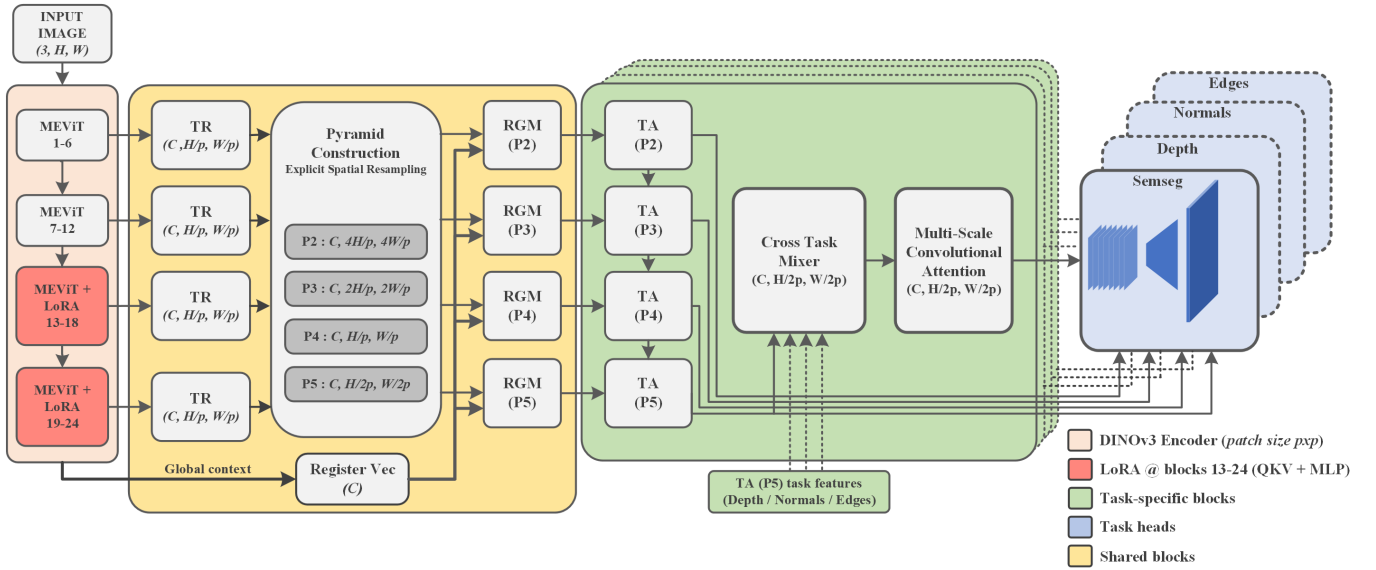


Fig. 2. Overview of M2H-MX. A monocular RGB image is processed by a DINOv3 encoder with Memory-Efficient Vision Transformer (MEViT) blocks and LoRA adaptation in the final transformer blocks. Token reassembly and pyramid construction form multi-scale features. Register-Gated Mamba (RGM) blocks inject global context from register tokens, while Task Adaptors (TA), Cross-Task Mixing (CTM), and Multi-Scale Convolutional Attention (MSCA) produce task-specific features for dense depth, semantic, normal, and edge prediction.

- We evaluate the resulting system against state-of-the-art monocular SLAM and reconstruction methods on ScanNet, addressing the lack of directly comparable monocular 3D scene graph baselines and demonstrating the downstream value of the proposed perception-to-mapping design.

## II. RELATED WORK

Dense multi-task learning has become a common approach for monocular scene understanding, as jointly predicting geometry and semantics allows complementary task cues to be shared across representations. Early methods such as MTI-Net [4] introduced structured feature exchange between depth and semantic segmentation, while transformer-based models such as InvPT [5] demonstrated the benefits of global context modeling for dense prediction. More recent work has explored efficiency-oriented designs that balance accuracy and computational cost, including state-space and sequence-based decoders such as MTMamba [6]. Within this line of research, M2H [7] showed that controlled cross-task interaction can improve monocular depth and semantic prediction while maintaining real-time performance. However, most existing multi-task models are evaluated primarily in isolation and are not explicitly designed for integration into a real-time monocular mapping pipeline.

In parallel, metric-semantic mapping systems combine geometric and semantic information to support higher-level spatial reasoning. Frameworks such as Kimera [2] and Hydra [3] produce structured spatial representations, including scene graphs, but typically assume depth sensing. Recent extensions to monocular input, such as Mono-Hydra [1], replace depth sensors with learned perception modules, making overall system performance strongly dependent on the quality, stability,

and runtime behavior of dense monocular perception. M2H-MX differs by designing the dense predictor around the latency, stability, and interface constraints of a fixed monocular mapping pipeline.

## III. METHODOLOGY

### A. M2H-MX Network

M2H-MX maps a monocular RGB frame to dense geometric and semantic predictions used by the downstream metric-semantic mapping pipeline. Its design follows four constraints: preserving strong foundation-model features, limiting trainable parameters, controlling cross-task interference, and maintaining real-time inference. Given an RGB image  $I_t \in \mathbb{R}^{3 \times H \times W}$ , the network predicts  $\{\hat{Y}_t^q\}_{q \in \mathcal{K}} = \text{M2H-MX}(I_t)$ , where  $\mathcal{K} = \{\text{depth, sem, norm, edge}\}$ . Depth and semantics are consumed by the mapping pipeline, while normals and edges provide auxiliary structural supervision.

For compact notation, Conv denotes convolution, Up and Pool denote spatial upsampling and downsampling, Reshape denotes map-token conversion,  $\sigma$  denotes the sigmoid function,  $\odot$  denotes elementwise multiplication, and  $*$  denotes convolution in prediction heads. As shown in Fig. 2, the architecture has four stages: backbone adaptation and feature pyramid construction, register-gated multi-scale decoding, task-specific cross-task refinement, and dense prediction heads. The resulting depth and semantic outputs are passed to the fixed VIO and mapping backend, where pose estimation and map fusion provide temporal alignment.

#### 1) Backbone Adaptation and Shared Feature Pyramid:

The first stage extracts dense features from a frozen DINOv3 encoder [8]. In Fig. 2, MEViT denotes the Memory-Efficient Vision Transformer blocks used inside the DINOv3 encoder. For input  $I_t$ , selected encoder layers  $\mathcal{L}$  produce hidden states

$\{H^\ell\}_{\ell \in \mathcal{L}}$ . Each  $H^\ell$  contains patch tokens  $H_{\text{patch}}^\ell \in \mathbb{R}^{N \times D}$ , where  $N = (H/p)(W/p)$  is the number of image patches,  $p$  is the patch size, and  $D$  is the encoder embedding dimension.

To adapt the frozen encoder with few trainable parameters, LoRA [9] is applied to the query-key-value (QKV) and multi-layer perceptron (MLP) projections of the final 12 transformer blocks. For a frozen projection  $W_0$ , LoRA uses

$$W_{\text{eff}} = W_0 + \lambda BA,$$

where  $A$  and  $B$  are trainable low-rank matrices and  $\lambda$  is a scaling factor. Thus, the pretrained backbone remains fixed while the final transformer blocks are adapted for dense prediction.

Patch tokens are converted into spatial maps using token reassembly (TR) and projected to a common channel dimension:

$$\begin{aligned} F^\ell &= \text{TR}(H_{\text{patch}}^\ell), \\ \tilde{F}^\ell &= \text{Conv}_{1 \times 1}^\ell(F^\ell). \end{aligned}$$

The selected reassembled features are fused into  $F_{\text{base}} = \Phi(\{\tilde{F}^\ell\}_{\ell \in \mathcal{L}})$ , where  $\Phi(\cdot)$  denotes convolution, normalization, activation, and feature aggregation. The pyramid construction block then forms the shared decoder pyramid:

$$\begin{aligned} p_4 &= \psi_4(F_{\text{base}}), & p_5 &= \psi_5(\text{Pool}(p_4)), \\ p_3 &= \psi_3(\text{Up}(p_4)), & p_2 &= \psi_2(\text{Up}(p_3)). \end{aligned}$$

Here,  $\psi_k$  is a scale-specific projection, while Pool and Up denote spatial downsampling and bilinear upsampling. This produces the shared pyramid  $\{p_2, p_3, p_4, p_5\}$ .

The final encoder layer also provides  $R$  register tokens  $\{h_{\text{reg},j}^{\text{last}}\}_{j=1}^R$ , shown as the ‘‘Register Vec’’ path in Fig. 2. These tokens are pooled into a compact global context vector

$$r = W_r \left( \frac{1}{R} \sum_{j=1}^R h_{\text{reg},j}^{\text{last}} \right),$$

which conditions all decoder scales with scene-level context.

We use DINOv3 because its Gram anchoring improves dense feature stability during large-scale self-supervised training, which is important for the spatially coherent patch features required by M2H-MX [8].

2) *Register-Gated Multi-Scale Decoder*: The second stage propagates information across pyramid scales using Register-Gated Mamba (RGM) blocks. At scale  $k \in \{5, 4, 3, 2\}$ , the pyramid feature is fused with the upsampled coarser decoder state and reshaped into a token sequence:

$$\begin{aligned} x_k &= p_k + \text{Up}(s_{k+1}; p_k), \\ q_k &= \text{Reshape}(x_k). \end{aligned}$$

Here,  $s_{k+1}$  is the decoder output from the next coarser pyramid level, and  $\text{Up}(s_{k+1}; p_k)$  upsamples it to the spatial resolution of  $p_k$  before fusion. At the coarsest level, we set  $s_6 = 0$ . The global register vector generates a channel gate,

$$\begin{aligned} g_k &= \sigma(\mathcal{A}_k(r)), \\ q_k^g &= q_k \odot g_k, \end{aligned}$$

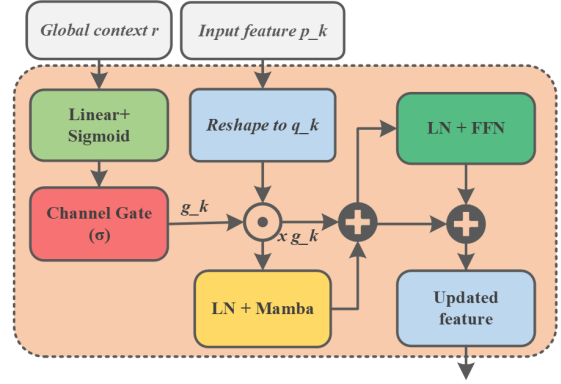


Fig. 3. Register-Gated Mamba (RGM) block used at each decoder scale. The global context vector  $r$  generates a channel gate  $g_k$  through a Linear+Sigmoid projection. The input feature is reshaped into  $q_k$ , modulated by  $g_k$ , and refined by LN+Mamba and LN+FFN residual branches to produce the updated feature.

where  $\mathcal{A}_k$  is a scale-specific linear projection and  $g_k$  is broadcast across spatial tokens. The gated sequence is then refined by a Mamba block [10] and a feed-forward network:

$$s_k = \text{Reshape}^{-1}(\text{RGM}_k(q_k, q_k^g)).$$

Here,  $s_k \in \mathbb{R}^{C \times H_k \times W_k}$  is the updated shared decoder feature at scale  $k$ , and the set  $\{s_2, s_3, s_4, s_5\}$  is passed to the task-adaptor blocks in the next stage. The notation  $\text{RGM}_k(q_k, q_k^g)$  summarizes the LN+Mamba and LN+FFN residual branches in Fig. 3;  $q_k^g$  provides global conditioning, while  $q_k$  is preserved through residual updates. LN denotes layer normalization and FFN denotes a feed-forward network.

3) *Task-Specific Cross-Task Refinement*: The third stage adapts the shared decoder features  $\{s_k\}_{k=2}^5$  into task-specific representations. Task adaptors (TA) convert these shared multi-scale features into branch-specific features  $h_\tau$  for each target task  $\tau$  before cross-task refinement. Cross-Task Mixing (CTM) then injects selected context features into a target branch:

$$\begin{aligned} z_j &= \Pi_j(h_j) \odot (1 + \sigma(G_j(h_j))), \\ u_\tau &= \text{Conv}_{1 \times 1}(\{h_\tau, \{z_j\}_{j \in \mathcal{C}_\tau}\}). \end{aligned}$$

Here,  $h_\tau$  is the target-task feature,  $h_j$  is a context-task feature,  $\mathcal{C}_\tau$  is the selected context set,  $\Pi_j$  aligns channels, and  $G_j$  predicts a gate. This task-directed design allows each branch to use complementary cues only where useful, instead of forcing all tasks to exchange information symmetrically.

The mixed feature  $u_\tau$  is refined by Multi-Scale Convolutional Attention (MSCA), which uses depthwise convolutions with multiple receptive fields to produce a spatial attention map  $A_{\text{spatial}}^\tau$ . The refined feature is

$$\tilde{h}_\tau = u_\tau + A_{\text{spatial}}^\tau \odot u_\tau.$$

MSCA emphasizes task-relevant local structures such as boundaries, planar regions, and thin objects. CTM followed by MSCA is applied to semantic, normal, and edge branches. The depth branch uses a dedicated bin-based head for adaptive metric calibration and residual refinement, while its feature can still serve as CTM context for the other branches.

4) *Task Heads*: The fourth stage converts refined task features into dense predictions. Depth is predicted with an adaptive bin-based head. Given the refined depth feature  $\tilde{h}_d$ , global average pooling predicts adaptive bin widths, while a per-pixel classifier predicts bin probabilities:

$$w = \text{softmax}(W_w * \text{GAP}(\tilde{h}_d)), \quad p_b = \text{softmax}(W_b * \tilde{h}_d).$$

The bin centers  $c_i$  are obtained by cumulatively summing the predicted bin widths  $w$  over the valid depth range. The final depth is

$$\hat{D} = \sum_{i=1}^{N_b} p_{b,i} c_i + W_o * \tilde{h}_d.$$

Here, GAP is global average pooling,  $N_b$  is the number of adaptive depth bins,  $p_{b,i}$  is the probability of bin  $i$  at each pixel, and  $W_o * \tilde{h}_d$  is the residual depth correction.

The semantic branch uses a lightweight convolutional classifier:

$$\hat{S} = \text{Conv}_{1 \times 1} \left( \delta(\text{Conv}_{3 \times 3}(\tilde{h}_s)) \right),$$

where  $\delta$  denotes the nonlinear activation. The normal and edge branches use lightweight dense heads:

$$\hat{N} = \text{NormHead}(\tilde{h}_n), \quad \hat{E} = \sigma(\text{EdgeHead}(\tilde{h}_e)).$$

5) *Loss Functions and Uncertainty-Based Balancing*: Each task  $q \in \mathcal{K}$  uses a main loss and auxiliary losses from decoder scales:

$$\mathcal{L}_q = \mathcal{L}_q^{\text{main}} + \sum_{k=2}^5 \alpha_{k,q} \mathcal{L}_{k,q}^{\text{aux}}.$$

The loss type follows the output: pixel-wise classification for semantics, dense regression for depth, angular or cosine loss for normals, and binary loss for edges. Auxiliary supervision encourages intermediate decoder features to remain task-relevant.

We also use consistency terms between geometrically related outputs:

$$\mathcal{L}_{\text{cons}} = \lambda_{dn} \mathcal{L}_{dn}(\hat{D}, \hat{N}) + \lambda_{se} \|\sigma(\hat{E}) - \phi(\hat{S})\|_1.$$

The first term encourages compatibility between predicted depth and normals, while the second aligns predicted edges with a semantic-boundary map  $\phi(\hat{S})$  computed from the predicted segmentation.

The full multi-task objective uses learned uncertainty weighting [11]:

$$\mathcal{L}_{\text{total}} = \sum_{q \in \mathcal{K}} \left( \frac{1}{2s_q^2} \mathcal{L}_q + \log s_q \right) + \mathcal{L}_{\text{cons}}.$$

Here,  $s_q$  is the learned uncertainty of task  $q$ . This reduces manual tuning of task weights by assigning lower effective weight to tasks with higher learned uncertainty, while the logarithmic term prevents unbounded growth of  $s_q$ .

## B. System Integration and Scope

Fig. 1 illustrates how M2H-MX is deployed within the Mono-Hydra monocular SLAM pipeline [1]. At runtime, M2H-MX replaces only the perception front end. It predicts dense depth and semantic labels from monocular RGB input; the predicted depth is combined with RGB to form RGB-D frames for inertial odometry, while semantic labels are used by the mapping backend for metric-semantic map construction and downstream scene graph generation. All state estimation, optimization, mapping, and scene graph construction modules are kept unchanged; therefore, the system-level differences reported in Sec. IV can be attributed to the proposed perception front end and its perception-to-mapping interface.

## IV. EXPERIMENTS

The experimental evaluation addresses three questions: (i) does M2H-MX improve dense multi-task prediction quality, (ii) do these improvements translate into measurable gains in a running monocular SLAM system, and (iii) which architectural components are responsible for these gains.

### A. Datasets and Metrics

We evaluate dense perception performance on NYUDv2 [12] and Cityscapes [13], and system-level behavior in a running monocular SLAM pipeline on ScanNet [14]. NYUDv2 and Cityscapes represent standard indoor and outdoor benchmarks for joint semantic and depth estimation, while ScanNet enables evaluation under realistic deployment conditions. Reported metrics include semantic mIoU, depth or disparity RMSE, and Absolute Trajectory Error (ATE) for SLAM evaluation.

### B. Implementation Details and Evaluation Protocol

Unless otherwise stated, experiments use M2H-MX-L with a DINOv3-ViT-L backbone, decoder width  $C = 256$ , Mamba state size 32, four register tokens, and 64 depth bins. M2H-MX-B differs only by using the shallower DINOv3-ViT-B backbone; the decoder, task heads, and training protocol remain unchanged. For M2H-MX-L, LoRA is applied to the final 12 backbone blocks ( $r = 16$ ,  $\alpha = 32$ , dropout 0.05), with all other backbone parameters frozen. Input resolution follows each dataset protocol.

For NYUDv2, all four heads (depth, semantics, normals, edges) are active. For Cityscapes evaluation and ScanNet deployment, only depth and semantics are enabled because these datasets do not provide the full set of normal and edge annotations needed to train and evaluate the auxiliary heads consistently. ScanNet experiments use a model trained on the ScanNet25k subset, on which it achieves 76.10 mIoU and 0.2210 depth RMSE. Evaluation sequences are not used for model selection. Runtime evaluation is performed on a workstation with an Intel i7-14700K CPU, 32GB DDR5 memory, and an NVIDIA RTX 4080 Super GPU. Perception runs asynchronously on the GPU, while state estimation and mapping run on the CPU.

TABLE I  
NYUDv2 DEPTH AND SEMANTICS RESULTS.

Method	Semseg mIoU $\uparrow$	Depth RMSE $\downarrow$
TaskPrompter [15]	55.30	0.5152
MQTransformer [16]	54.84	0.5325
MTMamba [6]	55.82	0.5066
InvPT-B MTPD-C [5], [17]	54.86	0.5150
MLoRE [18]	55.96	0.5076
MTMamba++ [19]	57.01	0.4818
M2H [7]	61.54	0.4196
M2H-MX-B	61.80	0.4170
<b>M2H-MX-L (this work)</b>	<b>65.60</b>	<b>0.3800</b>

TABLE II  
CITYSCAPES SEMANTIC AND DISPARITY RESULTS.

Method	Semseg mIoU $\uparrow$	Disparity RMSE $\downarrow$
MTI-Net [4]	59.85	5.06
InvPT [5]	71.78	4.67
TaskPrompter [15]	72.41	5.49
MTMamba [6]	78.00	4.66
MTMamba++ [19]	79.13	4.63
<b>M2H-MX-L (this work)</b>	<b>82.28</b>	<b>3.89</b>

### C. Dense Perception Benchmarks

We begin by comparing dense prediction quality on standard benchmarks to verify that M2H-MX improves per-frame depth and semantic estimates. We then test the same model inside a running monocular SLAM pipeline and ablate the main design blocks. Table I summarizes NYUDv2 results compared against representative multi-task learning baselines. M2H-MX-L improves both semantic and geometric accuracy, achieving the highest mIoU and the lowest depth RMSE among all compared methods.

Relative to M2H, the strongest compared baseline on NYUDv2, M2H-MX-L improves semantic mIoU by +4.06 points (61.54  $\rightarrow$  65.60) while reducing depth RMSE by approximately 9.4% (0.4196  $\rightarrow$  0.3800). These gains indicate that the proposed register-gated decoding and controlled cross-task interaction improve both prediction quality and cross-task consistency.

*Comparison scope.* Since several compared methods could not use DINOv3 [8] at the time they were developed, the NYUDv2 comparison should be interpreted as a complete M2H-MX configuration comparison rather than a backbone-controlled decoder comparison. The ablation in Table V therefore shows how much M2H-MX depends on the encoder choice.

Table II reports Cityscapes results. Compared with the strongest baseline, MTMamba++, M2H-MX-L improves semantic mIoU by +3.15 points (79.13  $\rightarrow$  82.28) while reducing disparity RMSE from 4.63 to 3.89. This demonstrates that the proposed design generalizes beyond indoor datasets and remains effective in large-scale outdoor scenes.

### D. Real-Time System Evaluation in SLAM

While dense benchmark performance is necessary, the primary objective of M2H-MX is stable deployment in a real-time monocular SLAM system. Table III reports model-level

TABLE III  
MODEL COMPLEXITY UNDER DIFFERENT ACTIVE-HEAD SETTINGS. GFLOPS ARE REPORTED AT THE EVALUATED INPUT RESOLUTION.

Method	#P (M)	GFLOPs
<i>Reported baselines</i>		
TaskPrompter [15]	373.00	416
MTMamba++ [19]	315.00	524
M2H [7]	81.00	488
<i>M2H-MX variants (this work)</i>		
M2H-MX-B (4 heads)	134.26	322.67
M2H-MX-L (2 heads)	332.03	371.76
M2H-MX-L (4 heads)	353.53	491.91

TABLE IV  
AVERAGE ATE [CM] ON SELECTED SCANNET SEQUENCES (LOWER IS BETTER).

Method	Avg. ATE [cm]
<i>RGB-D baselines</i>	
iMAP [20]	56.21
NICE-SLAM [21]	13.05
DROID-SLAM (VO) [22]	11.59
DROID-SLAM [22]	7.15
Go-SLAM [23]	7.02
<i>Monocular methods</i>	
DROID-SLAM (VO) [22]	63.61
DROID-SLAM [22]	52.60
Go-SLAM [23]	17.59
<b>Mono-Hydra stack [1] (with M2H-MX)</b>	<b>6.91</b>

profiling in terms of parameters and GFLOPs. Despite the additional task heads and cross-task refinement, the M2H-MX-L configuration requires 371.76 GFLOPs with the two active deployment heads, depth and semantics, and 491.91 GFLOPs with all four heads. In Mono-Hydra, the four-head deployment sustains 15–20 Hz in the asynchronous perception-to-mapping loop.

To evaluate downstream impact, Table IV reports average ATE on selected ScanNet sequences. All methods in Table IV are evaluated on the same selected ScanNet sequences. RGB-D methods are included as reference points, while the primary comparison is against monocular SLAM and reconstruction methods because M2H-MX uses only monocular RGB input at the sensor level. On the selected ScanNet sequences, M2H-MX reduces average ATE from 17.59 cm for monocular Go-SLAM to 6.91 cm. This result indicates that improved per-frame depth and semantic quality directly translates into more stable camera tracking and map construction.

Fig. 4 provides a qualitative comparison on ScanNet scene0054\_00, showing fewer visible reconstruction artifacts and more coherent metric–semantic structure than the monocular baselines.

### E. Ablation Study: Feature Quality vs. Decoder Complexity

Table V shows that M2H-MX gains arise from a deliberate balance between strong backbone features and lightweight decoding. Removing both CTM and MSCA reduces mIoU by 2.07 points and increases depth RMSE, while CTM-only and MSCA-only variants show limited benefit. Removing RGM or the register feed also degrades both semantics and depth, confirming the role of register-conditioned decoding.

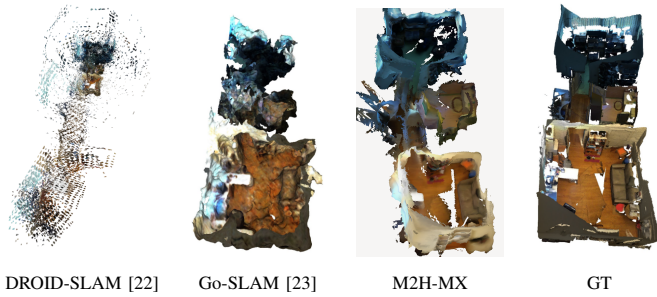


Fig. 4. Qualitative monocular mapping comparison on ScanNet scene0054\_00. Compared with DROID-SLAM and Go-SLAM, integrating M2H-MX produces fewer visible reconstruction artifacts and more coherent metric-semantic structure in the downstream map.

TABLE V  
ABLATION RESULTS ON NYUDV2 RELATIVE TO M2H-MX-L.

Variant	mIoU $\uparrow$	RMSE $\downarrow$	$\Delta$ mIoU	$\Delta$ RMSE
M2H-MX-L	65.60	0.3800	–	–
<i>Component ablations</i>				
No CTM/MSCA	63.53	0.4619	-2.07	+0.0819
CTM only	63.55	0.4705	-2.05	+0.0905
MSCA only	63.53	0.4575	-2.07	+0.0775
w/o RGM	64.44	0.4346	-1.16	+0.0546
w/o reg. feed	64.22	0.4473	-1.38	+0.0673
<i>Different backbones</i>				
DINOv2-L	56.79	0.5131	-8.81	+0.1331
ConvNeXt-L	38.83	0.6940	-26.77	+0.3140

*Backbone sensitivity.* Table V also shows that backbone feature quality matters. Replacing DINOv3 with ConvNeXt causes a large degradation, indicating that the decoder is designed for dense transformer features and global register context rather than generic convolutional features. DINOv2 performs better than ConvNeXt, but still reduces mIoU from 65.60 to 56.79 and increases RMSE from 0.3800 to 0.5131. This suggests that DINOv3 provides more suitable spatially coherent features, consistent with its Gram anchoring strategy [8]. This supports the intended design of M2H-MX as a decoder specialized for dense transformer features rather than a backbone-agnostic decoder.

## V. CONCLUSION

This paper presented M2H-MX, a deployment-oriented monocular perception model for real-time metric-semantic mapping and scene graph generation. By combining a frozen foundation-model backbone, lightweight adaptation, register-gated decoding, and controlled cross-task interaction, M2H-MX improves dense depth and semantic prediction under runtime constraints.

On NYUDv2, M2H-MX improves semantic mIoU by 4.06 points and reduces depth RMSE by 9.4% over the strongest compared multi-task baseline. In the fixed Mono-Hydra pipeline on ScanNet, it reduces average trajectory error from 17.59 cm to 6.91 cm, a 60.7% improvement, while producing cleaner metric-semantic maps. These results show that carefully designed multi-task perception can deliver measurable system-level gains when integrated through a compact perception-to-mapping interface.

## REFERENCES

- [1] U. Udugama, G. Vosselman, and F. Nex, "Mono-hydra real-time 3d scene graph construction from monocular camera input with imu," *ISPRS Annals of Photogrammetry, Remote Sensing and Spatial Information Sciences*, vol. X-1/W1-2023, pp. 439–445, 2023.
- [2] A. Rosinol, M. Abate, Y. Chang, and L. Carlone, "Kimera: an open-source library for real-time metric-semantic localization and mapping," in *ICRA*. IEEE, 2020, pp. 1689–1696.
- [3] N. Hughes, Y. Chang, and L. Carlone, "Hydra: A real-time spatial perception system for 3d scene graph construction and optimization," *arXiv preprint arXiv:2201.13360*, 2022.
- [4] S. Vandenhende, S. Georgoulis, and L. Van Gool, "Mti-net: Multi-scale task interaction networks for multi-task learning," in *ECCV*. Springer, 2020, pp. 527–543.
- [5] H. Ye and D. Xu, "Inverted pyramid multi-task transformer for dense scene understanding," in *ECCV*. Springer, 2022, pp. 514–530.
- [6] B. Lin, W. Jiang, P. Chen, Y. Zhang, S. Liu, and Y.-C. Chen, "Mtmamba: Enhancing multi-task dense scene understanding by mamba-based decoders," in *ECCV*. Springer, 2024, pp. 314–330.
- [7] U. Udugama, G. Vosselman, and F. Nex, "M2h: Multi-task learning with efficient window-based cross-task attention for monocular spatial perception," in *IROS*, 2025, pp. 8067–8072.
- [8] O. Siméoni, H. V. Vo, M. Seitzer, F. Baldassarre, M. Oquab, C. Jose, V. Khalidov, M. Szafraniec, S. Yi, M. Ramamonjisoa, F. Massa, D. Haziza, L. Wehrstedt, J. Wang, T. Darcet, T. Moutakanni, L. Sentana, C. Roberts, A. Vedaldi, J. Tolan, J. Brandt, C. Couprie, J. Mairal, H. Jégou, P. Labatut, and P. Bojanowski, "DINOv3," 2025.
- [9] E. J. Hu, Y. Shen, P. Wallis, Z. Allen-Zhu, Y. Li, S. Wang, L. Wang, and W. Chen, "Lora: Low-rank adaptation of large language models," in *International Conference on Learning Representations*, 2022.
- [10] A. Gu and T. Dao, "Mamba: Linear-time sequence modeling with selective state spaces," *arXiv preprint arXiv:2312.00752*, 2023.
- [11] A. Kendall, Y. Gal, and R. Cipolla, "Multi-task learning using uncertainty to weigh losses for scene geometry and semantics," in *Proceedings of the IEEE Conference on Computer Vision and Pattern Recognition*, 2018, pp. 7482–7491.
- [12] N. Silberman, D. Hoiem, P. Kohli, and R. Fergus, "Indoor segmentation and support inference from rgb-d images," in *European Conference on Computer Vision*. Springer, 2012, pp. 746–760.
- [13] M. Cordts, M. Omran, S. Ramos, T. Rehfeld, M. Enzweiler, R. Benenson, U. Franke, S. Roth, and B. Schiele, "The cityscapes dataset for semantic urban scene understanding," in *Proceedings of the IEEE Conference on Computer Vision and Pattern Recognition*, 2016, pp. 3213–3223.
- [14] A. Dai, A. X. Chang, M. Savva, M. Halber, T. Funkhouser, and M. Nießner, "ScanNet: Richly-annotated 3d reconstructions of indoor scenes," in *Proceedings of the IEEE conference on computer vision and pattern recognition*, 2017, pp. 5828–5839.
- [15] H. Ye and D. Xu, "Taskprompter: Spatial-channel multi-task prompting for dense scene understanding," in *ICLR*, 2023.
- [16] Y. Xu, X. Li, H. Yuan, Y. Yang, and L. Zhang, "Multi-task learning with multi-query transformer for dense prediction," *IEEE Transactions on Circuits and Systems for Video Technology*, vol. 34, no. 2, pp. 1228–1240, 2024.
- [17] Y. Shang, D. Xu, G. Liu, R. R. Kompella, and Y. Yan, "Efficient multitask dense predictor via binarization," in *CVPR*, 2024, pp. 15 899–15 908.
- [18] Y. Yang, P.-T. Jiang, Q. Hou, H. Zhang, J. Chen, and B. Li, "Multi-task dense prediction via mixture of low-rank experts," in *CVPR*, 2024, pp. 27 927–27 937.
- [19] B. Lin, W. Jiang, P. Chen, S. Liu, and Y.-C. Chen, "Mtmamba++: Enhancing multi-task dense scene understanding via mamba-based decoders," *IEEE Transactions on Pattern Analysis and Machine Intelligence*, 2025.
- [20] E. Sucar, S. Liu, J. Ortiz, and A. Davison, "iMAP: Implicit mapping and positioning in real-time," in *Proceedings of the International Conference on Computer Vision (ICCV)*, 2021.
- [21] Z. Zhu, S. Peng, V. Larsson, W. Xu, H. Bao, Z. Cui, M. R. Oswald, and M. Pollefeys, "Nice-slam: Neural implicit scalable encoding for slam," in *Proceedings of the IEEE/CVF Conference on Computer Vision and Pattern Recognition (CVPR)*, 2022.
- [22] Z. Teed and J. Deng, "DROID-SLAM: Deep Visual SLAM for Monocular, Stereo, and RGB-D Cameras," *Advances in neural information processing systems*, 2021.

- [23] Y. Zhang, F. Tosi, S. Mattocchia, and M. Poggi, “Go-slam: Global optimization for consistent 3d instant reconstruction,” in *Proceedings of the IEEE/CVF International Conference on Computer Vision (ICCV)*, October 2023.